

HURRICANE SANDY BEFORE 1900 AND AFTER 2100

BY GARY M. LACKMANN

If the synoptic pattern accompanying Sandy had occurred in the past or if it were to repeat in the future, how would the storm differ in response to climate change?

On 29 October 2012, Hurricane Sandy was reclassified as “posttropical” prior to a dramatic landfall in the southern portion of the state of New Jersey in the U.S. mid-Atlantic region, eventually resulting in \$50 billion estimated damage (Blake et al. 2013). Sandy’s track at landfall was nearly perpendicular to the coastline, which is climatologically unusual for this region (Hall and Sobel 2013). In the aftermath of the event, questions arose concerning the possible contribution of climate warming to the track and intensity of the storm. Some investigators hypothesize that climate warming increases the frequency of blocking patterns in the jet stream, resulting in a greater likelihood of storm tracks similar to that of Sandy (Francis and Vavrus 2012). Other investigators find a decrease in the frequency of steering flows conducive to tracks similar to that

of Sandy as a result of climate warming (Barnes et al. 2013). While attribution of individual extreme weather events such as Sandy to climate change is fundamentally problematic, meaningful questions can be posed: 1) How does climate change affect the frequency or intensity of events similar to Hurricane Sandy? 2) If the large-scale synoptic weather pattern associated with Sandy had taken place in the past or if it were repeated in the future, would the track and/or intensity of the system differ appreciably from what was observed because of thermodynamic changes?

Although question 1) is of great importance, it is more difficult to answer. Further, answering 2) contributes uniquely to understanding of the relation between extreme weather and climate change by isolating storm-scale changes due to alterations in the larger-scale thermodynamic environment. The methods used to answer this question are also fairly straightforward and have been tested in a variety of applications (e.g., Schär et al. 1996; Kawase et al. 2009; Lynn et al. 2009; Rasmussen et al. 2011; Lackmann 2013; Mallard et al. 2013a,b; Yates et al. 2014). First, we establish hypotheses regarding how and why one would expect climate change to affect the track and intensity of Sandy, and then we utilize a suite of numerical simulations to test these hypotheses for a time period beginning in the middle of Sandy’s life cycle.

Hurricane Sandy exhibited many of the classic features of a tropical cyclone (TC) but, during the time period leading up to landfall, the system interacted

AFFILIATIONS: LACKMANN—Department of Marine, Earth, and Atmospheric Sciences, North Carolina State University, Raleigh, North Carolina

CORRESPONDING AUTHOR: Gary M. Lackmann, Department of Marine, Earth and Atmospheric Sciences, North Carolina State University, 1125 Jordan Hall, Box 8208, Raleigh, NC 27695
E-mail: gary@ncsu.edu

The abstract for this article can be found in this issue, following the table of contents.

DOI:10.1175/BAMS-D-14-00123.1

In final form 30 July 2014

©2015 American Meteorological Society

strongly with midlatitude weather systems (Galarneau et al. 2013), including an upper-level trough/ridge system embedded within the jet stream, as well as two frontal systems in the lower troposphere (Fig. 1a). The cloud band to the east of Sandy corresponded to an analyzed warm front; the meridional cloud band to the west of Sandy, over eastern North America, coincided with a cold front (Fig. 1a); the analysis of Galarneau et al. (2013) emphasizes the importance of lower-tropospheric frontal baroclinic processes as contributing to the secondary peak in storm intensity as Sandy approached landfall. Satellite imagery and numerical model experiments illustrate that in the upper troposphere, anticyclonic outflow from Sandy contributed to the strength of the downstream ridge that was centered over the Canadian Maritime provinces prior to and during Sandy's landfall (Fig. 1b); anticyclonic flow associated with this upper ridge likely contributed to the westward steering of Sandy toward the New Jersey shore (Fig. 2). Had this ridge been weaker, Sandy may have turned harmlessly eastward into the North Atlantic. The upper-level trough located to the south of Sandy also contributed to the westward track of Sandy (e.g., Galarneau et al. 2013; Magnusson et al. 2014), and satellite imagery indicates that outflow from Sandy also overlapped with the northern portion of this trough (Fig. 1b).

A known consequence of climate warming is an increase in atmospheric water vapor content (e.g., Allen and Ingram 2002). With constant relative humidity, warming increases vapor capacity,

resulting in vapor increases in approximate agreement with the Clausius–Clapeyron equation (Pall et al. 2007). For this reason, an increase in the occurrence of heavy precipitation is expected with a warming climate (e.g., Trenberth et al. 2003; Pall et al. 2007). Numerical studies indicate heavier rainfall in simulations of future tropical cyclones as well (e.g., Knutson et al. 2010). A dynamical consequence of this thermodynamic change is increased condensational heating, which could drive stronger tropical cyclones. However, additional factors, such as a warming maximum in the tropical upper troposphere, partially compensate for this effect (e.g., Knutson and Tuleya 1999, 2004; Shen et al. 2000; Knutson et al. 2001; Hill and Lackmann 2011). While this upper-level tropical warming maximum is a robust feature of general circulation model (GCM) simulations, observations have not revealed a clear indication of this phenomenon (Santer et al. 2005; Po-Chedley and Fu 2012). If increased condensational heating were to occur in a storm such as Sandy, this could also alter synoptic-scale steering features, such as the downstream, upper-level anticyclone, as discussed above (Henderson et al. 1999; Torn 2010). Has sufficient warming and moistening taken place to allow intensification of the upper-level anticyclone that contributed to Sandy's westward track? One hypothesis is that warming and moistening strengthened the downstream ridge via increased condensational heating (beyond what would have been observed in preindustrial times), which in turn drove Sandy more strongly westward.

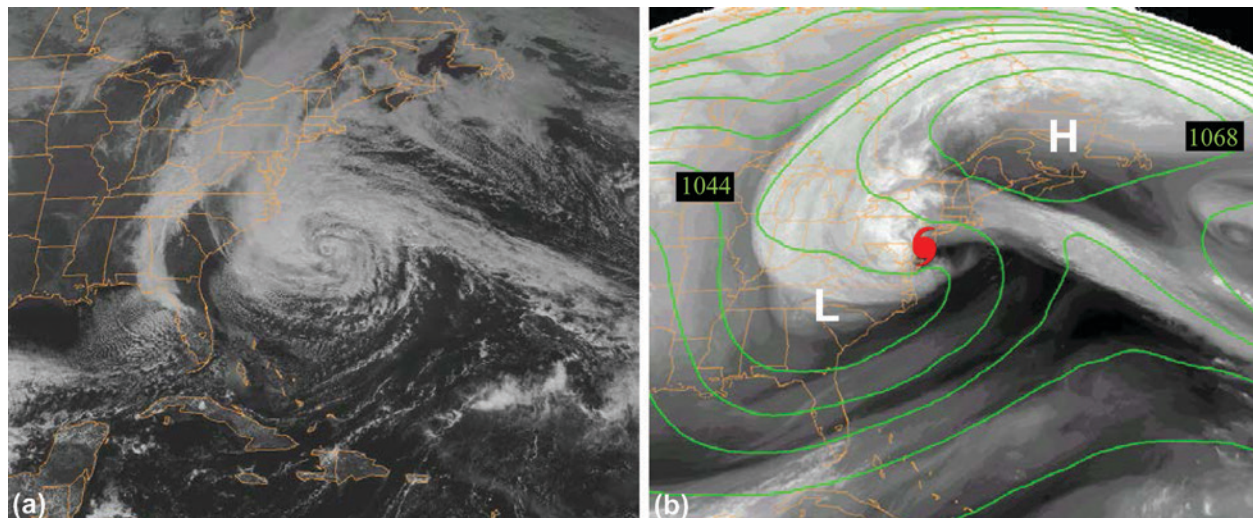


FIG. 1. Geostationary Operational Environmental Satellite-13 (GOES-13) satellite imagery: (a) visible image for 1745 UTC 28 Oct 2012 and (b) water vapor image for 2345 UTC 29 Oct 2012, with 0000 UTC 20 Oct 2012 European Centre for Medium-Range Weather Forecasts (ECMWF) interim reanalysis 250-hPa geopotential height [green contours: interval of 12 decameters (dam); 1044- and 1068-dam contours labeled] to illustrate locations of upper-tropospheric cyclone and anticyclone. The red hurricane symbol indicates the location of Sandy.

For a tropical cyclone moving northward along the U.S. East Coast, this argument predicts a more southerly landfall location under current conditions relative to what would have happened in the past for a given initial synoptic pattern.

However, the upper-level anticyclone to the north of Sandy was not the only steering influence. Because of a warming maximum in the tropical upper troposphere, larger absolute humidity increases in the tropics relative to higher latitudes, and other factors, climate warming leads to an increase in the strength of the westerly jet stream (e.g., Yin 2005; Lorenz and DeWeaver 2007). A strengthening westerly jet under climate warming would lead to a different prediction from that suggested by the previous hypothesis in two ways. First, a strengthened westerly jet would add to the eastward steering flow. Second, the upper wave pattern described previously would tend to be more progressive in the presence of a stronger jet. These processes would contribute to a more easterly track of a storm like Sandy, resulting in a more northward landfall location with future warming. With sufficient jet strengthening, the storm could move into the North Atlantic and perhaps avoid a North American landfall altogether. Finally, as noted in reference to Fig. 1b, the outflow from Sandy also affected the upper-level trough located to the southwest of Sandy, and this would have the effect of weakening the trough through diabatic processes. A weaker trough to the south of Sandy would in turn serve to lessen the westward steering flow component. Numerical experiments are required to determine which, if any, of these hypothesized effects dominates.

METHODS. A set of numerical model simulations was produced using the Weather Research and Forecasting (WRF) Model (Skamarock et al. 2007); WRF has proven capable in the analysis and prediction of tropical cyclones (e.g., Davis et al. 2008; Munsell and Zhang 2014; Bassill 2014, 2015). A summary of varia-



FIG. 2. Sea level pressure (yellow contours; 4-hPa interval) from 54-km control run, with 300-hPa wind speed difference (vector arrows) between a full-physics model simulation and a simulation in which the effects of condensational heating were withheld, valid at 0000 UTC 30 Oct 2012. This time corresponds to hour 96 of the model simulations, which were initialized at 0000 UTC 26 Oct. The center of the upper-level anticyclonic perturbation flow is marked with an H, and the red hurricane symbol indicates the location of Sandy.

tions in resolution, physical parameterizations, and initial conditions is provided in Table 1. All simulations presented here utilized initial and boundary condition data obtained from the European Centre for Medium-Range Weather Forecasts (ECMWF) interim reanalysis (Dee et al. 2011), available with an approximate grid length of 0.7°. The selection of initialization time for this study reflects a balance between the need for accurate current-climate track simulation and sufficient lead time to allow differences to evolve. A previous analysis of ensemble forecasting system performance for this event by Munsell and Zhang (2014) found that forecasts initialized at 0000 UTC 26 October 2012 exhibited considerable track sensitivity and that a subset of ensemble members tracked the system out to sea. Although the results of Bassill (2014, 2015) demonstrate greater track sensitivity at earlier initial times, track results for current-climate simulations initialized earlier (e.g., 0000 UTC 24 October) do not verify as favorably as those for simulations initialized at 0000 UTC 26 October. Furthermore, the track changes in response to warming from earlier-initialized simulations (0000 UTC 24 October) are consistent with those from 0000 UTC 26 October (not shown). The current-climate ensemble presented here, initialized

TABLE I. Summary of all WRF Model experiments presented or discussed: WRF Model version 3.2.1 was used for the simulations included below, except for runs I5DFI and I7, which used WRF3.6. The DFI run designation indicates use of digital filter initialization. The climate column designates past (P), current (C), and future (F) simulations. The cumulus parameterization (CP) scheme choices included Kain–Fritsch (KF), Betts–Miller–Janjić (BMJ), Tiedtke (T), and none (0). The microphysics (MP) column choices included the WRF single-moment 6-class microphysics scheme (WSM6), the Goddard scheme, the WRF double-moment 6-class microphysics scheme (WDM6), the Morrison scheme, and a simulation with no MP heating. The initial condition (IC) time designates the time of model initialization, either 0000 UTC 26 Oct (for most runs) or 0000 UTC 24 Oct (for runs I6 and I7). The planetary boundary layer (PBL) and TC flux column includes use of the Yonsei University (YSU) scheme and the Mellor–Yamada–Janjić (MYJ) scheme, and all but run I utilized the TC flux correction option. All simulations used vertical motion damping, 50 dry-air sigma model levels, and set a model top of 50 hPa.

Run	Climate	Grid length (km)	CP scheme	Microphysics	IC time	PBL/TC flux
I	P, C, and F	54, 18, 6	KF, KF, none	WSM6	0000 UTC 26 Oct	YSU/no
2	P, C, and F	54, 18, 6	KF, KF, none	WSM6	0000 UTC 26 Oct	YSU/yes
3	P, C, and F	54, 18, 6	KF, KF, none	Goddard	0000 UTC 26 Oct	YSU/yes
4	P, C, and F	54, 18, 6	KF, KF, none	WDM6	0000 UTC 26 Oct	YSU/yes
5	P, C, and F	54, 18, 6	KF, KF, none	Morrison	0000 UTC 26 Oct	YSU/yes
6	P, C, and F	54, 18, 6	BMJ, BMJ, none	WSM6	0000 UTC 26 Oct	MYJ/yes
7–II	F (GCM)	54, 18, 6	KF, KF, none	WSM6	0000 UTC 26 Oct	YSU/yes
I3	C	54, 18, 6	None	No MP heat	0000 UTC 26 Oct	YSU/yes
I4DFI	P, C, and F	54	KF	WSM6	0000 UTC 26 Oct	YSU/yes
I5DFI	P, C, and F	54, 18, 6	KF, KF, none	WSM6	0000 UTC 26 Oct	YSU/yes
I6	P, C, and F	54	KF, KF, none	WSM6	0000 UTC 24 Oct	YSU/yes
I7	C and F	54, 18, 6	T, T, none	WSM6	0000 UTC 24 Oct	YSU/yes

at 0000 UTC 26 October 2012, provides an adequate depiction of the observed track (Fig. 3a). Although the ensemble-mean track did not extend as far east as the observed storm on 28 October, prior to landfall, the ensemble-mean simulated landfall was within 15 km of the observed location. Despite an initial central pressure that was approximately 20 hPa too high (because of the coarse resolution of the initial data), the current ensemble produces a reasonable replication of the observed intensity, with minimum central pressure at landfall matching the observed 940 hPa (Fig. 3b). To test the hypotheses described above, high-resolution simulations are required in order to capture the full intensity of the tropical cyclone as well as the expected process interactions (Gentry and Lackmann 2010). The ability of the current ensemble to adequately represent Sandy's track and intensity in a multiday simulation leading up to landfall bolsters confidence in the ability of the model to represent the relevant physical processes in this case. Ensembles of 18 members with varying resolution and model physical parameterization are used to obtain a more robust solution than could be obtained by comparing individual simulations.

The simulations were run with grid lengths of 54, 18, and 6 km, with one-way nesting for the inner two domains.

Large-scale climate changes between the 1880s and 2010s were computed using coarse-grained gridded data obtained from a subset of five GCMs that were used in the Intergovernmental Panel on Climate Change (IPCC) Fourth Assessment Report (AR4), available as part of phase 3 of the Coupled Model Intercomparison Project (CMIP3; Meehl et al. 2007). Climate change was computed using GCM output from the following centers: Bjerknes Center for Climate Research [Bergen Climate Model, version 2.0 (BCCR-BCM2.0)], Centre National de Recherches Météorologiques [Coupled Global Climate Model, version 5 (CNRM-CM3)], Institute for Numerical Mathematics [Coupled Model, version 3.0 (INM-CM3.0)] Max-Planck Institut für Meteorologie (ECHAM5), and the Met Office (UKMO). These models were selected based on the availability of data for both the twentieth-century and future projections. Monthly-mean data for October were further averaged over a 10-yr period from 1880 to 1890. A similar procedure was used for the period from 2000 to 2010.

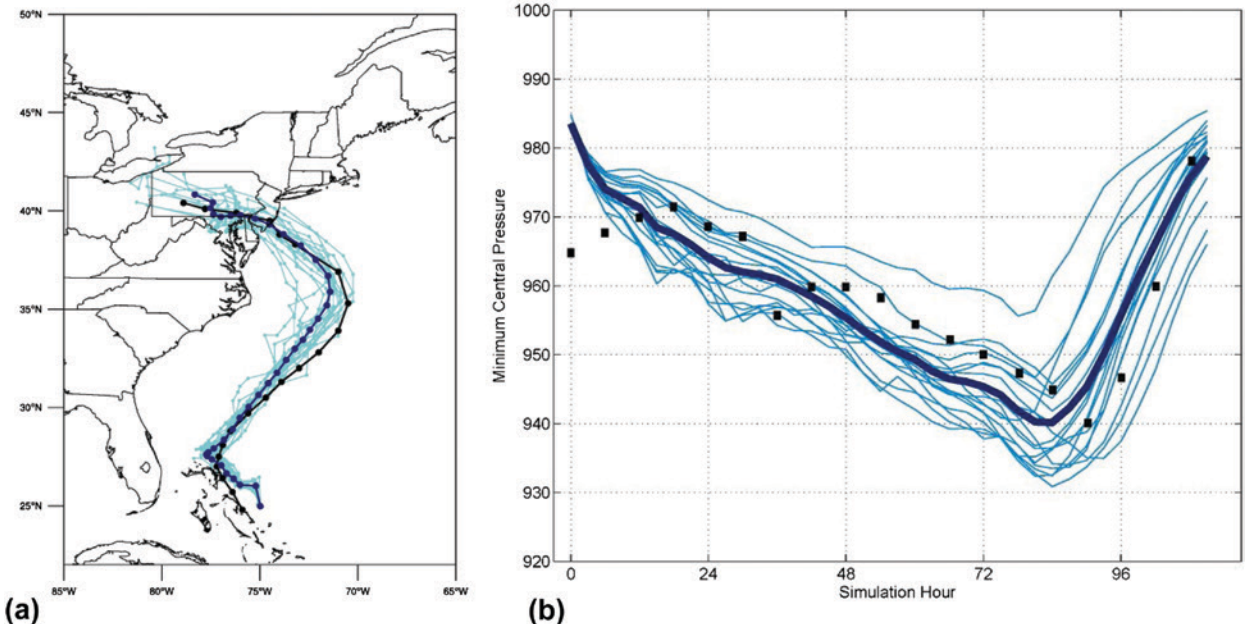


FIG. 3. Current ensemble comparison to observations for (a) track and (b) intensity. Black line in (a) and black boxes in (b) correspond to National Hurricane Center best-track observations (Blake et al. 2013). Thicker blue line depicts ensemble mean.

Difference fields were then computed for all relevant thermodynamic quantities, including sea surface temperature, 2-m air temperature, surface and soil temperatures, and air temperature at all available vertical levels. The temperature changes provided the basis for computing changes in specific humidity and geopotential height. Change fields (Figs. 4a,b) were then vertically interpolated and subtracted from the same ECMWF initial and lateral boundary data used for the current simulations, and the ensemble was rerun using an identical configuration. This ensemble loosely represents a “historic version” of Hurricane Sandy, corresponding to large-scale thermodynamic conditions roughly 120 years ago, but with a synoptic weather pattern highly reminiscent of that from late October 2012. Some model fields, such as land use, were not altered, but this is not expected to have an important influence on these 6-day simulations. Following the application of temperature and moisture changes, the hydrostatically balanced geopotential field was computed. Because of the large amount of averaging involved, changes in horizontal geopotential gradients were smooth enough to allow the model wind field to adjust to the modified geopotential field upon integration; GCM-derived wind field changes were not applied to the initial conditions. Tests undertaken using the WRF digital filter initialization (DFI) procedure (Lynch and Huang 1992, 1994; Chen and Huang 2006, see

Table 1), which fully balances the wind fields at the initial time using an adiabatic backward and diabatic forward integration, produced tracks that were highly similar to those in the simulations in which the DFI procedure was not used (not shown).

Finally, initial and boundary conditions for a future version of Sandy were generated using methods similar to those used to create the past simulations. For this, data obtained from the same aforementioned subset of five IPCC GCMs were used. The more recent CMIP5 data are available (Taylor et al. 2012); however, the large-scale temperature changes between the CMIP3 and CMIP5 are remarkably similar (e.g., Knutti and Sedláček 2012, their Figs. 1, 2). Thermodynamic change fields were based on the A2 emissions scenario and differences were calculated between the 1990s and the 2090s (Figs. 4c,d). These change fields were again applied to the initial and boundary conditions used in the current simulations, this time to generate “future” versions of Sandy, corresponding roughly to projected thermodynamic conditions 100 years in the future. The procedure for computing temperature, moisture, geopotential, and wind field changes was identical to that described above for the past changes. Changes between the 1880s and 2010s were more modest than the projected changes from the 1990s to the 2090s (Fig. 4). The spatial structure of the moisture change depicted in Fig. 4d indicates greater moistening in warm air, consistent with the Clausius–Clapeyron relation under

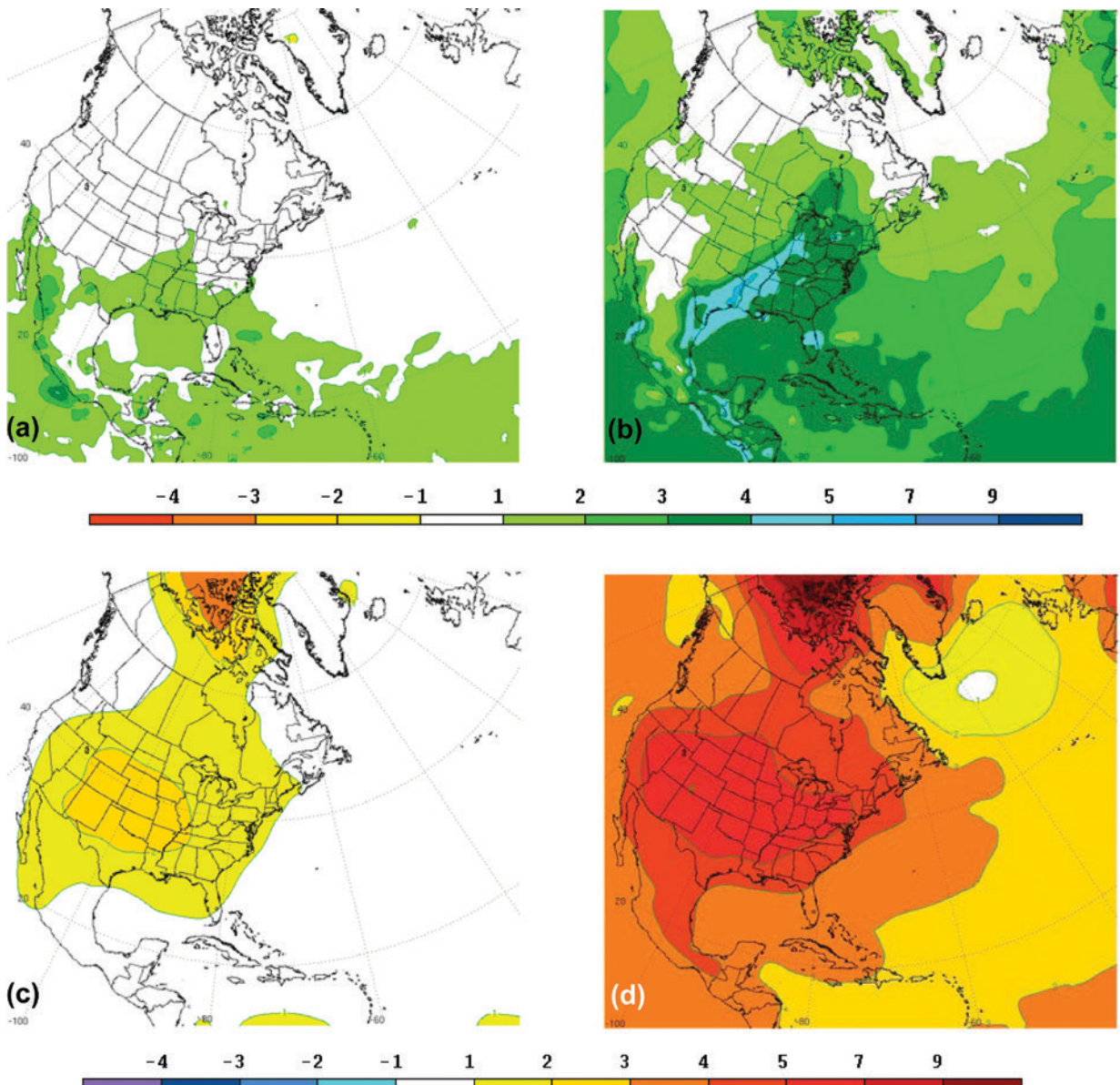


FIG. 4. Change fields obtained from GCM ensemble, applied to simulation initial conditions: (a) current minus past and (b) future minus current 2-m water vapor mixing ratio change (g kg^{-1} ; shaded as in legend) and (c) current minus past and (d) future minus current temperature change (K; shaded as in legend).

warming conditions. While this moisture effect can locally enhance geopotential gradients, tests with the DFI again demonstrated limited sensitivity of initial wind field adjustments to this aspect. To test sensitivity to varying GCM solutions, the future ensemble was supplemented with five additional simulations that utilized change fields from the individual GCMs.

RESULTS. The ensemble-mean track for the historic version of Sandy indicates landfall at a location approximately 100 km south-southwest of the observed location (Figs. 5a, 6). The past ensemble of simulations yields an average intensity that is

~ 5 hPa weaker than the current ensemble at landfall. However, a paired *t* test demonstrates that the difference in ensemble-mean pressure is not significant at the 95% confidence level, leading to the conclusion that the imposed thermodynamic changes produced only a modest influence on the intensity of Sandy. Although the track changes are also modest, the consistency of the change among ensemble members suggests that the effect of increased jet strength or greater diabatic weakening of the trough to the southwest of Sandy in the current simulations may have dominated that due to changes in the intensity of the downstream upper-tropospheric ridge in these simulations.

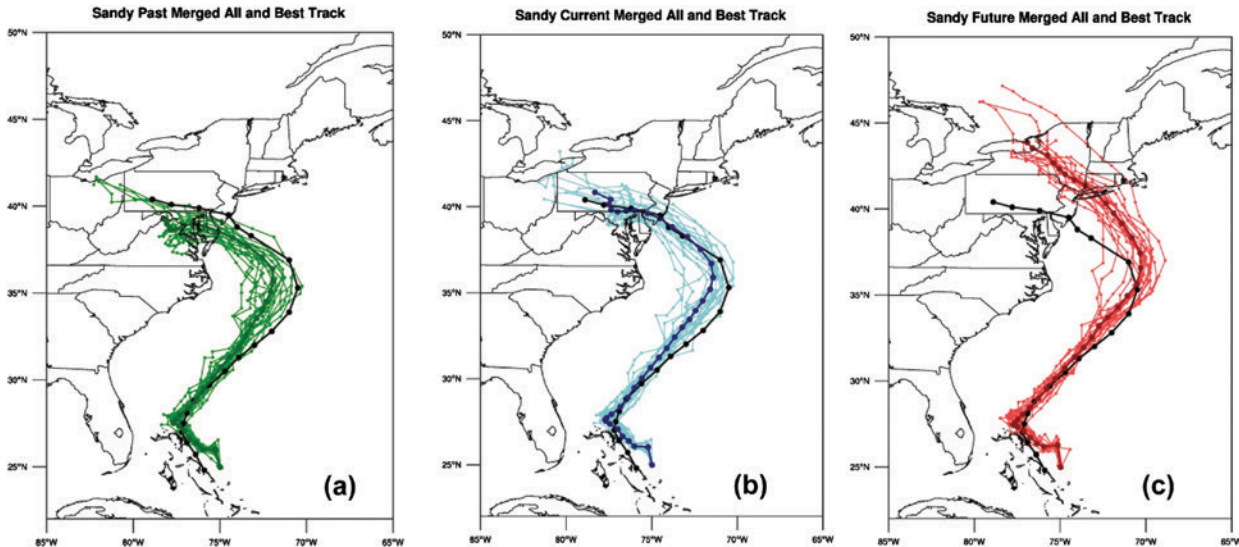


FIG. 5. Track ensembles for (a) past, (b) current, and (c) future paths of Hurricane Sandy, derived from 6-day WRF simulations initialized 0000 UTC 26 Oct. The black line represents the National Hurricane Center best track; lighter colored lines represent ensemble members, and darker colored lines represent ensemble means for past (green), current (blue), and future (red).

The future ensemble-mean track follows the current track until the point where the observed Sandy made a sharp westward turn; subsequent to that point, on 29 October, the future ensemble tracks more gradually northwestward, making landfall more than 200 km north-northeast of the observed location, in the vicinity of Long Island, New York (Figs. 5c, 6). The future ensemble intensity is substantially greater, with an average minimum central pressure at landfall more than 10 hPa lower than for the current ensemble and observed storm (Fig. 7c). A paired *t* test demonstrates that the future intensity increase is statistically significant at 95% confidence. The future strengthening is evident even early in the simulations (Fig. 7d) and is not attributable to changes in landfall timing. The more northward landfall location in the future ensemble suggests that the strengthening of the westerly jet stream and diabatic weakening of the trough to the southwest of Sandy dominate over strengthening of the downstream outflow ridge in steering Sandy.

As a means of assessing the variability associated with change fields computed from individual GCM projections, an additional set of 15 simulations in which changes from the individual GCMs, rather than the average, were used to perturb the initial analyses. The full set of future ensemble members, including these additional simulations, indicates that increased

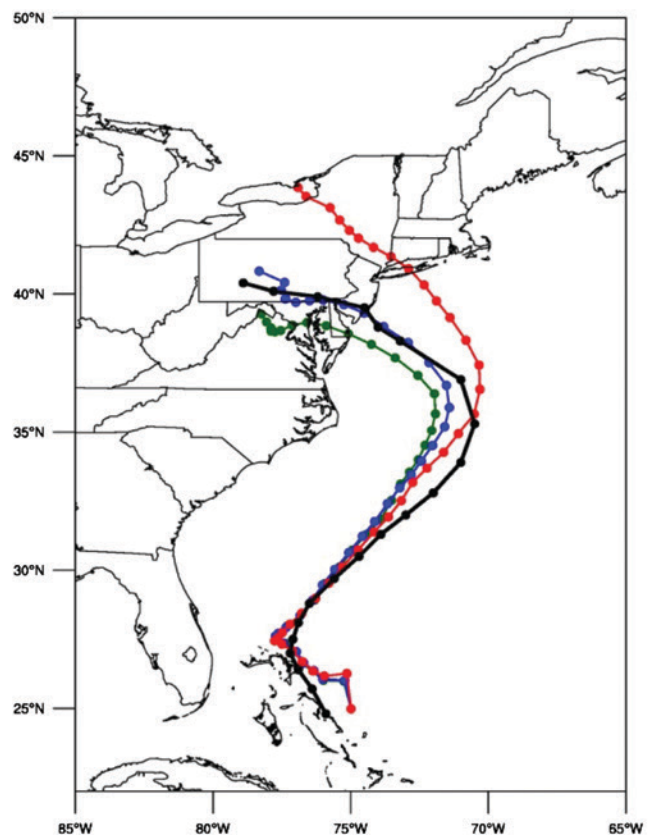


FIG. 6. Track comparison for overall 18-member ensemble means (combining 54-, 18-, and 6-km simulations for each time period) for 6-day model simulations. Past (green), current (blue), and future (red) are shown along with the National Hurricane Center best track (black).

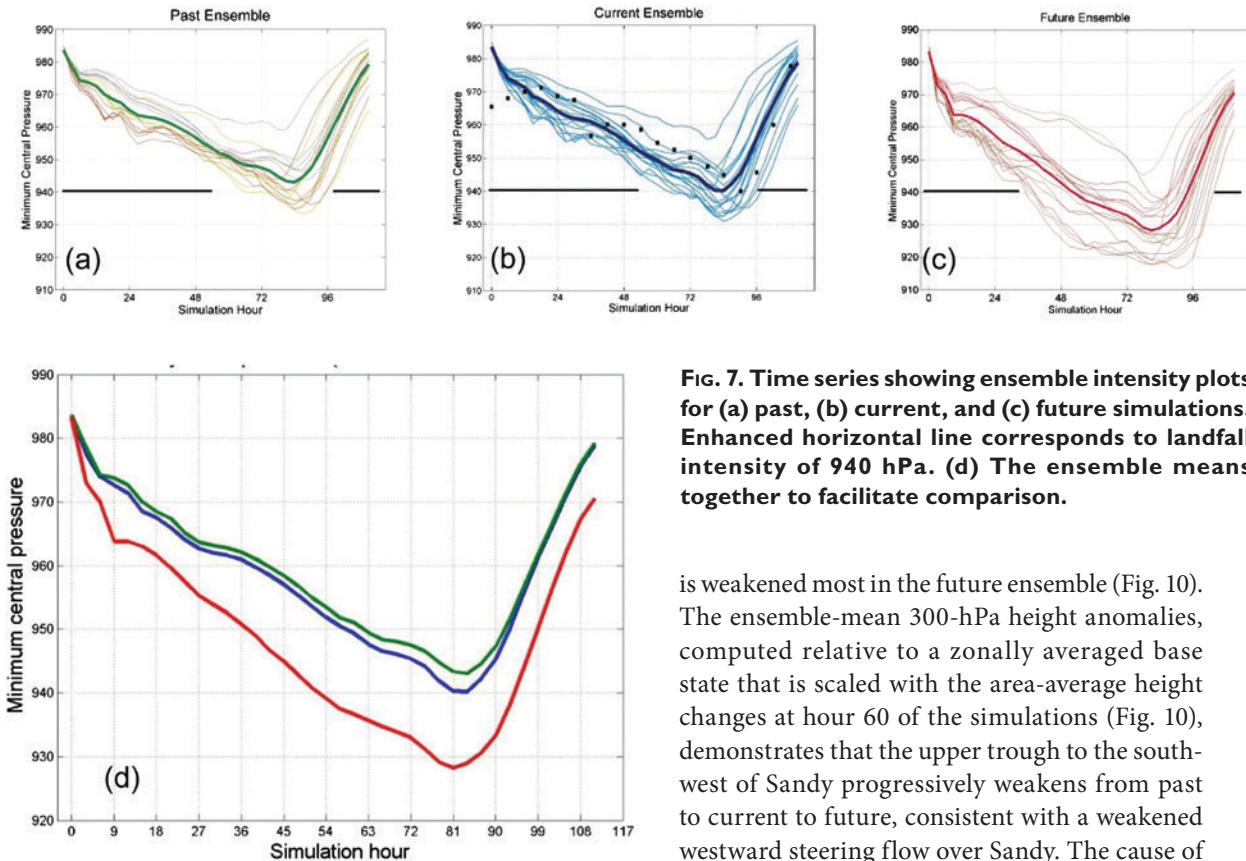


FIG. 7. Time series showing ensemble intensity plots for (a) past, (b) current, and (c) future simulations. Enhanced horizontal line corresponds to landfall intensity of 940 hPa. (d) The ensemble means together to facilitate comparison.

ensemble spread is evident but that the mean is nearly unchanged from that in the initial future ensemble (Fig. 8).

To explain the simulated track and intensity changes, ensemble-mean and temporal averages were computed and analyzed. Cross sections through the potential vorticity (PV) tower associated with Sandy (not shown) indicate that a cyclonic PV maximum greater than 4 PVU ($1 \text{ PVU} = 10^{-6} \text{ K kg}^{-1} \text{ m}^2 \text{ s}^{-1}$) extends vertically to between the 250- and 450-hPa levels, suggesting that flow changes at the 300-hPa level could be useful in analysis of track changes; Munsell and Zhang (2014) indicate that a lower steering level may be more relevant. A difference field, future minus current, of 300-hPa geopotential height and wind demonstrates that the strengthened future westerly jet is potentially responsible for the future track change (Fig. 9a). Although 300-hPa geopotential height rises everywhere in future relative to current simulations, the northern portion of the future upper trough to the northwest of Sandy results in lessened rises there, producing an increase in westerly flow across the path of Sandy during the time of northward storm movement in the western North Atlantic (Fig. 9a). In conjunction, the southern portion of the trough, located to the southwest of Sandy,

is weakened most in the future ensemble (Fig. 10). The ensemble-mean 300-hPa height anomalies, computed relative to a zonally averaged base state that is scaled with the area-average height changes at hour 60 of the simulations (Fig. 10), demonstrates that the upper trough to the southwest of Sandy progressively weakens from past to current to future, consistent with a weakened westward steering flow over Sandy. The cause of this weakening is likely increased condensational heating in the future ensemble, consistent with enhanced water vapor content, rainfall, and the larger lower-tropospheric PV shown in Fig. 9b.

The greater future storm intensity is consistent with increased water vapor and heavier rainfall in the future simulation. This can be quantified via plots of the lower-tropospheric PV (Fig. 9b), which can be viewed as an integrated measure of the dynamical influence of condensational heating. The future simulation produces the strongest ensemble-mean lower-tropospheric cyclonic PV maximum, consistent with greater tropical cyclone intensity and with previous studies (e.g., Hill and Lackmann 2011). The baroclinic intensification mechanism presented by Galarneau et al. (2013) for this case may have been modified by the more northward track relative to the Gulf Stream in the future simulations. However, differences in future versus current intensity were evident well before Sandy approached the Gulf Stream boundary.

CONCLUSIONS. The results of a set of high-resolution numerical simulations, utilizing change fields computed from a subset of five IPCC AR4 GCM projections, demonstrate that large-scale thermodynamic change can influence the track and intensity of Hurricane Sandy even within the limits

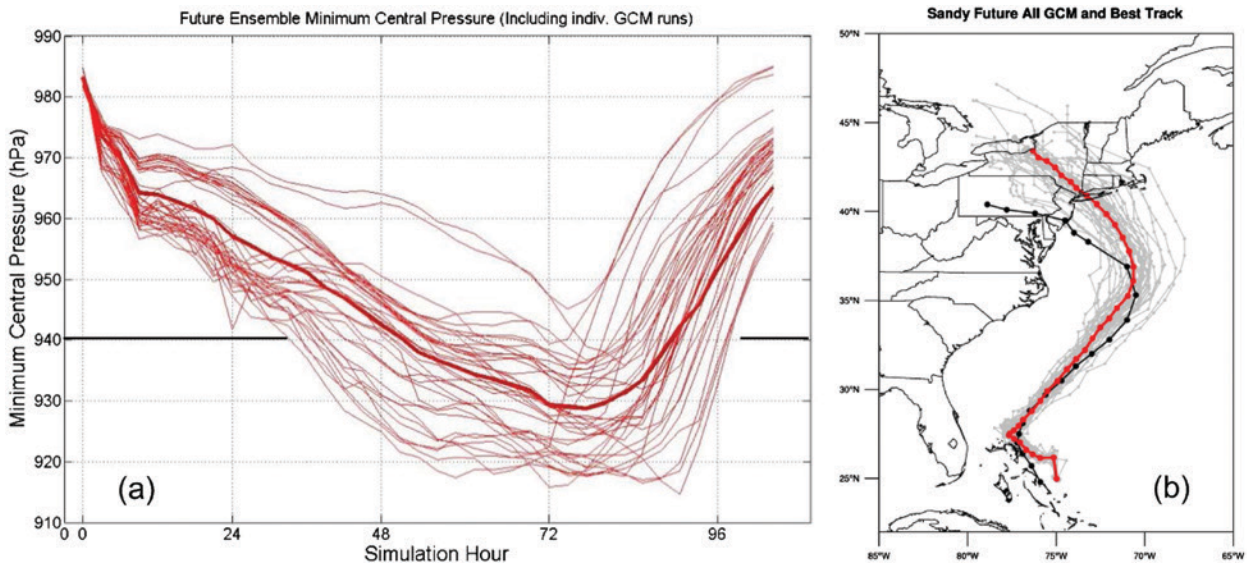


FIG. 8. As in Fig. 7, but for future ensemble including additional members obtained by utilizing individual GCM changes in altering initial conditions: (a) minimum central pressure and (b) track.

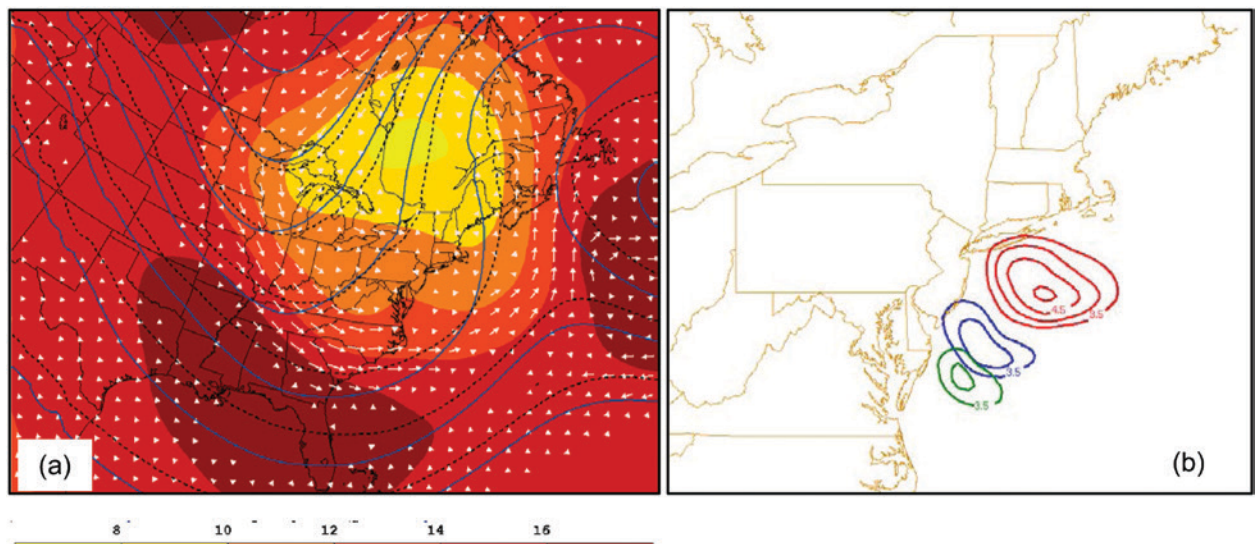


FIG. 9. Ensemble-mean analysis: (a) 300-hPa geopotential height difference (future minus current; shaded as in legend below panel) and corresponding vector wind difference (white vector arrows), superimposed with current and future 300-hPa height (12-dam interval; blue and dashed black contours, respectively). Data are time-averaged between 1200 UTC 26 Oct and 0000 UTC 28 Oct. (b) Ensemble-mean potential vorticity (contour interval 0.5 PVU) at hour 84 of the simulations for past (green), current (blue), and future (red).

imposed by a highly similar initial synoptic weather pattern. However, there are several important caveats regarding the methods employed in this study that are pertinent to conclusions about the impacts of a storm like Sandy in the past and future. First, thermodynamic changes were applied at a midway point in the evolution of Sandy, and changes in the

evolution of Sandy leading up to this point have not been accounted for.¹ The question as to whether Sandy would have even formed in a different climate has not been addressed, and previous studies have demonstrated sensitivity of TC genesis to the thermodynamic environment (e.g., Emanuel et al. 2008; Rappin et al. 2010; Mallard et al. 2013a,b).

¹ Shen et al. (2013) analyze the predictability of Sandy's genesis using a global mesoscale model; future research into the climate impacts on Sandy's genesis would be insightful.

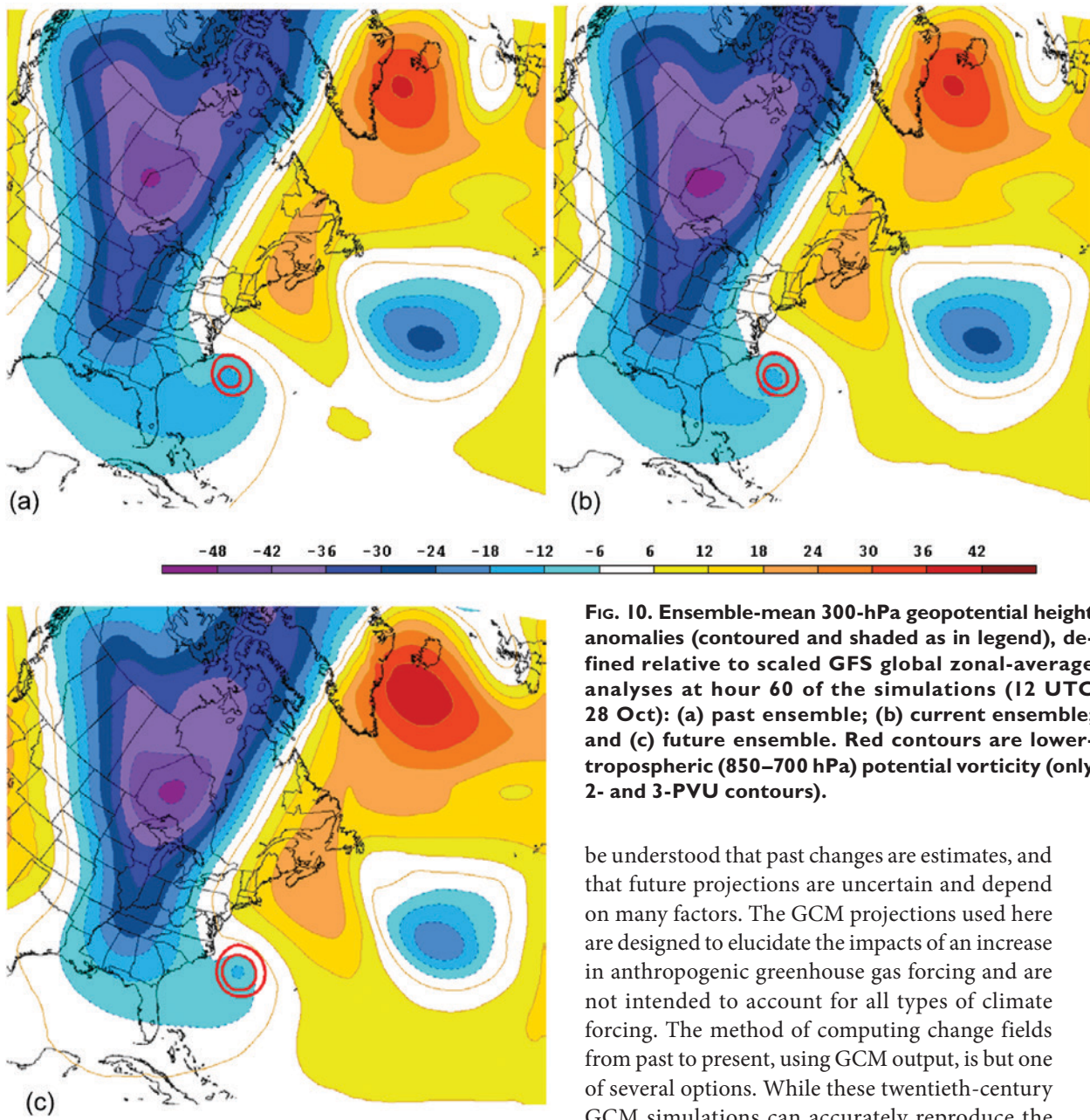


FIG. 10. Ensemble-mean 300-hPa geopotential height anomalies (contoured and shaded as in legend), defined relative to scaled GFS global zonal-average analyses at hour 60 of the simulations (12 UTC 28 Oct): (a) past ensemble; (b) current ensemble; and (c) future ensemble. Red contours are lower-tropospheric (850–700 hPa) potential vorticity (only 2- and 3-PVU contours).

Differences between past, current, and future simulations would likely be amplified with longer integrations. Second, this study does not address changes in the frequency of this type of synoptic pattern. Third, the techniques employed here ignore the influence of sea level rise, which certainly exacerbated Sandy's impact in the present day and would do so even more with future warming. Likewise, land-use changes and coastal development and population growth undoubtedly increased vulnerability and the severity of societal impacts during the observed Hurricane Sandy relative to what would have happened in the past. Finally, it must

be understood that past changes are estimates, and that future projections are uncertain and depend on many factors. The GCM projections used here are designed to elucidate the impacts of an increase in anthropogenic greenhouse gas forcing and are not intended to account for all types of climate forcing. The method of computing change fields from past to present, using GCM output, is but one of several options. While these twentieth-century GCM simulations can accurately reproduce the global surface temperature trends during the simulation period, there is considerable uncertainty in regional changes. Future work will utilize alternate datasets, including the more recent CMIP5 GCM data, and explore different initialization times.

Nevertheless, within the limits of the methods used, we conclude that had the synoptic pattern accompanying Hurricane Sandy during recurvature taken place prior to 1900, a slightly weaker storm and a more southerly landfall location would have resulted. The intensification is not statistically significant, indicating that thermodynamic changes to date did not contribute substantially to the observed strength of Sandy, given a similar synoptic evolution

from an initial point midway through the storm's trajectory.

Future simulations of Sandy are produced by modifying the model initial conditions to account for GCM-projected late-century thermodynamic changes derived from the IPCC AR4 A2 emissions scenario. These simulations reveal significant strengthening, and a more northward landfall location. The track shift is attributable to a weakening of the trough to the south of Sandy, a more progressive trough to the north, and a resulting increase in westerly flow over the path of Sandy as it moved northward parallel to the U.S. East Coast. An ensemble-mean decrease in central pressure of more than 10 hPa is found in the future ensemble, indicating that a future incarnation of Sandy would be substantially stronger. In conjunction with continuing sea level rise and coastal development, a future landfall of a stronger Sandy would have the potential to exert a much greater societal and economic impact than did the present-day Sandy. Numerous previous studies have found that climate warming can result in intensity increases for the strongest tropical cyclones (e.g., Emanuel 1987; Knutson and Tuleya 1999, 2004; Shen et al. 2000; Knutson et al. 2001; Emanuel et al. 2008; Knutson et al. 2010; Hill and Lackmann 2011). The results presented here are consistent with these earlier studies, despite the fact that Sandy was undergoing an extratropical transition during the pre-landfall period.

ACKNOWLEDGMENTS. This work was supported by NSF Grant 1007606, awarded to North Carolina State University. The WRF Model is made available by NCAR, funded by the National Science Foundation. The Program for Climate Model Diagnosis and Intercomparison (PCMDI) is acknowledged for collecting, archiving, and providing the CMIP3 model output, along with the WCRP's Working Group on Coupled Modelling (WGCM). The WCRP CMIP3 multimodel dataset is supported by the Office of Science, U.S. Department of Energy. Drs. Nick Bassill, Tom Galarneau, Walt Robinson, and Ed Zipser and an anonymous reviewer provided valuable feedback on earlier versions of this manuscript.

REFERENCES

- Allen, M. R., and W. J. Ingram, 2002: Constraints on future changes in climate and the hydrologic cycle. *Nature*, **419**, 224–232, doi:10.1038/nature01092.
- Barnes, E. A., L. M. Polvani, and A. H. Sobel, 2013: Model projections of atmospheric steering of Sandy-like superstorms. *Proc. Natl. Acad. Sci. USA*, **110**, 15 211–15 215, doi:10.1073/pnas.1308732110.
- Bassill, N. P., 2014: Accuracy of early GFS and ECMWF Sandy (2012) track forecasts: Evidence for a dependence on cumulus parameterization. *Geophys. Res. Lett.*, **41**, 3274–3281, doi:10.1002/2014GL059839.
- , 2015: An analysis of the operational GFS simplified Arakawa Schubert parameterization within a WRF framework: A Hurricane Sandy (2012) long-term track forecast perspective. *J. Geophys. Res. Atmos.*, **120**, 378–398, doi:10.1002/2014JD022211.
- Blake, E. S., T. B. Kimberlain, R. J. Berg, J. P. Cangialosi and J. L. Beven II, 2013: Tropical cyclone report: Hurricane Sandy. National Hurricane Center Rep. AL182012, 157 pp.
- Chen, M., and X.-Y. Huang, 2006: Digital filter initialization for MM5. *Mon. Wea. Rev.*, **134**, 1222–1236, doi:10.1175/MWR3117.1.
- Davis, C., and Coauthors, 2008: Prediction of land-falling hurricanes with the advanced hurricane WRF Model. *Mon. Wea. Rev.*, **136**, 1990–2005, doi:10.1175/2007MWR2085.1.
- Dee, D. P., and Coauthors, 2011: The ERA-Interim reanalysis: Configuration and performance of the data assimilation system. *Quart. J. Roy. Meteor. Soc.*, **137**, 553–597, doi:10.1002/qj.828.
- Emanuel, K. A., 1987: The dependence of hurricane intensity on climate. *Nature*, **326**, 483–485, doi:10.1038/326483a0.
- , R. Sundararajan, and J. Williams, 2008: Hurricanes and global warming: Results from downscaling IPCC AR4 simulations. *Bull. Amer. Meteor. Soc.*, **89**, 347–367, doi:10.1175/BAMS-89-3-347.
- Francis, J. A., and S. J. Vavrus, 2012: Evidence linking Arctic amplification to extreme weather in mid-latitudes. *Geophys. Res. Lett.*, **39**, L06801, doi:10.1029/2012GL051000.
- Galarneau, T. J., C. A. Davis, and M. A. Shapiro, 2013: Intensification of Hurricane Sandy (2012) through extratropical warm core seclusion. *Mon. Wea. Rev.*, **141**, 4296–4321, doi:10.1175/MWR-D-13-00181.1.
- Gentry, M. S., and G. M. Lackmann, 2010: Sensitivity of simulated tropical cyclone structure and intensity to horizontal resolution. *Mon. Wea. Rev.*, **138**, 688–704, doi:10.1175/2009MWR2976.1.
- Hall, T. M., and A. H. Sobel, 2013: The impact angle of Hurricane Sandy's New Jersey landfall. *Geophys. Res. Lett.*, **40**, 2312–2315, doi:10.1002/grl.50395.
- Henderson, J., G. M. Lackmann, and J. R. Gyakum, 1999: An analysis of Hurricane Opal's forecast track using quasigeostrophic potential vorticity inversion. *Mon. Wea. Rev.*, **127**, 292–307, doi:10.1175/1520-0493(1999)127<0292:AOHOS>2.0.CO;2.
- Hill, K. A., and G. M. Lackmann, 2011: The impact of future climate change on TC intensity and structure:

- A downscaling approach. *J. Climate*, **24**, 4644–4661, doi:10.1175/2011JCLI3761.1.
- Kawase, H., T. Yoshikane, M. Hara, F. Kimura, T. Yasunari, B. Ailikun, H. Ueda, and T. Inoue, 2009: Intermodel variability of future changes in the Baiu rainband estimated by the pseudo global warming downscaling method. *J. Geophys. Res.*, **114**, D24110, doi:10.1029/2009JD011803.
- Knutson, T. R., and R. E. Tuleya, 1999: Increased hurricane intensities with CO₂-induced warming as simulated using the GFDL hurricane prediction system. *Climate Dyn.*, **15**, 503–519, doi:10.1007/s003820050296.
- , —, 2004: Impact of CO₂-induced warming on simulated hurricane intensity and precipitation: Sensitivity to the choice of climate model and convective parameterization. *J. Climate*, **17**, 3477–3495, doi:10.1175/1520-0442(2004)017<3477:IOCWOS>2.0.CO;2.
- , —, W. Shen, and I. Ginis, 2001: Impact of CO₂-induced warming on hurricane intensities as simulated in a hurricane model with ocean coupling. *J. Climate*, **14**, 458–2468, doi:10.1175/1520-0442(2001)014<2458:IOCIWO>2.0.CO;2.
- , —, and Coauthors, 2010: Tropical cyclones and climate change. *Nat. Geosci.*, **3**, 157–163, doi:10.1038/ngeo779.
- Knutti, R., and J. Sedláček, 2012: Robustness and uncertainties in the new CMIP5 climate model projections. *Nat. Climate Change*, **3**, 369–373, doi:10.1038/nclimate1716.
- Lackmann, G. M., 2013: The south-central U.S. flood of May 2010: Present and future. *J. Climate*, **26**, 4688–4709, doi:10.1175/JCLI-D-12-00392.1.
- Lorenz, D. J., and E. T. DeWeaver, 2007: Tropopause height and zonal wind response to global warming in the IPCC scenario integrations. *J. Geophys. Res.*, **112**, D10119, doi:10.1029/2006JD008087.
- Lynch, P., and X.-Y. Huang, 1992: Initialization of the HIR-LAM model using a digital filter. *Mon. Wea. Rev.*, **120**, 1019–1034, doi:10.1175/1520-0493(1992)120<1019:IOTHMU>2.0.CO;2.
- , —, 1994: Diabatic initialization using recursive filters. *Tellus*, **46A**, 583–597, doi:10.1034/j.1600-0870.1994.t01-4-00003.x.
- Lynn, B. H., R. Healy, and L. M. Druyan, 2009: Investigation of Hurricane Katrina characteristics for future warmer climates. *Climate Res.*, **39**, 75–86, doi:10.3354/cr00801.
- Magnusson, L., J.-R. Bidlot, S. T. K. Lang, A. Thorpe, N. Wedi, and M. Yamaguchi, 2014: Evaluation of medium-range forecasts of Hurricane Sandy. *Mon. Wea. Rev.*, **142**, 1962–1981, doi:10.1175/MWR-D-13-00228.1.
- Mallard, M. S., G. M. Lackmann, A. Aiyyer, and K. A. Hill, 2013a: Atlantic hurricanes and climate change. Part I: Experimental design and isolation of thermodynamic effects. *J. Climate*, **26**, 4876–4893, doi:10.1175/JCLI-D-12-00182.1.
- , —, and —, 2013b: Atlantic hurricanes and climate change. Part II: Role of thermodynamic changes in decreased hurricane frequency. *J. Climate*, **26**, 8513–8528, doi:10.1175/JCLI-D-12-00183.1.
- Meehl, G. A., C. Covey, K. E. Taylor, T. Delworth, R. J. Stouffer, M. Latif, B. McAvaney, and J. F. B. Mitchell, 2007: The WCRP CMIP3 multimodel dataset: A new era in climate change research. *Bull. Amer. Meteor. Soc.*, **88**, 1383–1394, doi:10.1175/BAMS-88-9-1383.
- Munsell, E. B., and F. Zhang, 2014: Prediction and uncertainty of Hurricane Sandy (2012) explored through a real-time cloud-permitting ensemble analysis and forecast system assimilating airborne Doppler radar observations. *J. Adv. Model. Earth Syst.*, **6**, 38–58, doi:10.1002/2013MS000297.
- Pall, P., M. R. Allen, and D. A. Stone, 2007: Testing the Clausius-Clapeyron constraint on changes in extreme precipitation under CO₂ warming. *Climate Dyn.*, **28**, 351–363, doi:10.1007/s00382-006-0180-2.
- Po-Chedley, S., and Q. Fu, 2012: Discrepancies in tropical upper tropospheric warming between atmospheric circulation models and satellites. *Environ. Res. Lett.*, **7**, doi:10.1088/1748-9326/7/4/044018.
- Rappin, E. D., D. S. Nolan, and K. A. Emanuel, 2010: Thermodynamic control of tropical cyclogenesis in environments of radiative-convective equilibrium with shear. *Quart. J. Roy. Meteor. Soc.*, **136**, 1954–1971, doi:10.1002/qj.706.
- Rasmussen, R., and Coauthors, 2011: High-resolution coupled climate runoff simulations of seasonal snowfall over Colorado: A process study of current and warmer climate. *J. Climate*, **24**, 3015–3048, doi:10.1175/2010JCLI3985.1.
- Santer, B. D., and Coauthors, 2005: Amplification of surface temperature trends and variability in the tropical atmosphere. *Science*, **309**, 1551–1556, doi:10.1126/science.1114867.
- Schär, C., C. Frei, D. Lüthi, and H. C. Davies, 1996: Surrogate climate-change scenarios for regional climate models. *Geophys. Res. Lett.*, **23**, 669–672, doi:10.1029/96GL00265.
- Shen, B.-W., M. DeMaria, J.-L. F. Li, and S. Cheung, 2013: Genesis of Hurricane Sandy (2012) simulated with a global mesoscale model. *Geophys. Res. Lett.*, **40**, 4944–4950, doi:10.1002/grl.50934.
- Shen, W., R. E. Tuleya, and I. Ginis, 2000: A sensitivity study of the thermodynamic environment on GFDL model hurricane intensity: Implications for global

- warming. *J. Climate*, **13**, 109–121, doi:10.1175/1520-0442(2000)013<0109:ASSOTT>2.CO;2.
- Skamarock, W. C., J. B. Klemp, J. Dudhia, D. O. Gill, D. M. Barker, W. Wang, and J. G. Powers, 2007: A description of the Advanced Research WRF version 2. NCAR Tech. Note NCAR/TN-468+STR, 88 pp.
- Taylor, K. E., R. J. Stouffer, and G. A. Meehl, 2012: An overview of CMIP5 and the experiment design. *Bull. Amer. Meteor. Soc.*, **93**, 485–498, doi:10.1175/BAMS-D-11-00094.1.
- Torn, R. D., 2010: Diagnosis of the downstream ridging associated with extratropical transition using short-term ensemble forecasts. *J. Atmos. Sci.*, **67**, 817–833, doi:10.1175/2009JAS3093.1.
- Trenberth, K. E., A. Dai, R. M. Rasmussen, and D. B. Parsons, 2003: The changing character of precipitation. *Bull. Amer. Meteor. Soc.*, **84**, 1205–1217, doi:10.1175/BAMS-84-9-1205.
- Yates, D., B. Luna, R. Rasmussen, D. Bratcher, L. Garre, F. Chen, M. Tewari, and P. Friis-Hansen, 2014: Stormy weather: Assessing climate change hazards to electric power infrastructure: A Sandy case study. *IEEE Power Energy Mag.*, **12**, 66–75, doi:10.1109/MPE.2014.2331901.
- Yin, J. H., 2005: A consistent poleward shift of the storm tracks in simulations of 21st century climate. *Geophys. Res. Lett.*, **32**, L18701, doi:10.1029/2005GL023684.

Professional Quality at an Affordable Price



Vantage ProTM

Wireless and Cabled Weather Stations

Available from Davis Instruments, Vantage Pro2 weather stations offer reliable, professional-level accuracy and durability. Provides details on temperature, barometric pressure, wind, rain, humidity and dewpoints. Add optional consoles, stations and sensors for even more detailed information.

- Long wireless range to 1,000 ft.
- Frequent weather updates every 2.5 seconds
- Alarm settings for over 70 parameters
- Over 80 graphs for highs, lows, and totals



www.davisnet.com • 1-800-678-3669

BAM1504



TROPICS TO POLES DES TROPIQUES AUX POLES

ADVANCING SCIENCE IN HIGH LATITUDES

AVANCEMENT DE LA SCIENCE DES HAUTES LATITUDES

Abstract submission deadline: Feb 15th, 2015 Date limite pour la soumission des résumés: 15 février 2015

Early bird registration deadline April 18th, 2015 Date limite pour les inscriptions hâtives: 18 avril 2015



49th CMOS CONGRESS

13th AMS CONFERENCE ON POLAR METEOROLOGY AND OCEANOGRAPHY

49^{ème} CONGRÈS SCMO

13th AMS CONFERENCE ON POLAR METEOROLOGY AND OCEANOGRAPHY



2015 WHISTLER

May 31 - June 4

31 mai - 4 juin

British Columbia, Canada



Canadian Meteorological and Oceanographic Society
La Société canadienne de météorologie et d'océanographie

American Meteorological Society

www.congress.cmos.ca

[twitter:@CMOS2015](#)

Graphic designed by / Le graphique a été créé par : Helen Sun Vancouver, BC